# POPULATION-SPECIFIC EVALUATION OF IMPLANT BONE FITTING USING PCA SHAPE SPACE AND LEVEL SETS

*Nina Kozic[1], Miguel Á. González Ballester[2], Philippe Büchler[1],*
*Nils Reimers[3], Lutz P. Nolte[1], Marius G. Linguraru[4], Mauricio Reyes[1]*

[1] ARTORG Center for Biomedical Engineering Research, University of Bern, Switzerland
[2] Alma IT Systems, Barcelona, Spain
[3] Stryker Trauma GmbH, Kiel, Germany
[4] Radiology and Imaging Sciences, National Institutes of Health, Bethesda, MD, USA

## ABSTRACT

Currently in orthopedic research, bone shape variability within a specific population has been seldom investigated and used to optimise implant design, which is commonly performed by evaluating implant bone fitting on a limited dataset. In this paper, we extend our method for optimisation in statistical shape space, to global assessment of population-specific implant bone fitting. The method is based on a level set segmentation approach, used on the parametric space of the statistical shape model of the target population. The method highlights which patterns of bone variability are more important for implant fitting, allowing and easing implant design improvements. Results are presented for proximal human tibia.

***Index Terms***— statistical shape models, image registration, principal component analysis, level sets, implant fitting

## 1. INTRODUCTION

Currently, in orthopaedic research, the evaluation of implants for fracture fixation is done by manual fitting and fixation procedures, applied on a small set of cadaver bones in a trial-end-error process to find the optimal implant shape and position. This result can be greatly disrupted, since limited amount of cadaver specimens does not necessarily describe the diversity in a population, such as age, gender or ethnic origin. This diversity can be studied using statistical shape analysis techniques which are shown to be an efficient tool to build population specific model of anatomical variability. Its flagship, the Active Shape Model (ASM), proposed by Cootes et al. [1] provides a method to study the structure of a population of point data sets or meshes, decomposing the variability encountered across the population in a compact representation. This decomposition is obtained via principal components analysis (PCA) [2].

Statistical shape models representing the variation of the shape and gray-level appearance, namely Active Appearance Models (AAM) [3], have been extensively used in image segmentation to locate the structures of interest and to solve many medical image interpretation problems [3, 4, 5]. In all these cases, the aim is to find a single instance in the statistical shape model that best approximates the input data, subject to some regularisation constraints. In certain cases, it may be interesting to find *all* instances of the shape model that meet a criterion. For example, one may be interested in estimating which range of the population falls within a given anatomical

criterion, thus establishing a partition of the shape space into "valid" and "invalid" shapes. In [6] we propose a method for global optimisation of shape constraints, that effectively finds all instances in the PCA shape space that meet a given anatomical/morphological criterion.

In this work we apply the method proposed in [6] to the optimisation of implant bone fitting. We are able to find the group of instances that satisfy given fitting criterion and based on their correlation to the PCA manifold propose modifications to implant shape design as to fit a maximum of the target population.

The method is based on level sets on the parametric domain of the shape model. Level set methods define a powerful optimization framework that in combination with statistical shape prior can be used to recover objects of interest by propagating curves or surfaces [7, 8, 9]. However, these works are of very different nature to ours, as they deal with the extraction of structures of interest in medical images and modelling of shape prior knowledge in the level set space. In this work, level set approach will help in segmentation of a shape space of high-dimensionality, determined by the number of retained principal components. Moreover, the ability to represent complex topologies can be used to identify disconnected subsets of the shape space that meet the criterion.

Section 2 will introduce the basic concepts behind statistical shape models based on PCA. In section 3, we briefly overview the key idea, that is the use of level set segmentation for PCA shape space optimisation. In section 4 we apply our method to implant fitting of the human tibia. Finally, conclusions and future work are provided in section 5.

## 2. STATISTICAL SHAPE MODEL

### 2.1. Image registration

The first step in generating statistical model comprises the selection of an image from the training data set, as the reference/template bone. To compensate for the different positioning during CT acquisition, we align the remaining images of the training data set with the selected reference. The alignment is done by rigid registration to overcome the pose disparity and to maintain the size variation of the tibia. The next step in our model construction consists in warping the instances in the training set to the reference image. Image transformation is applied to each voxel of the training set of images to map them to the voxels inside the region of interest defined by the segmented reference image.

To capture the entire anatomical variability, we apply an
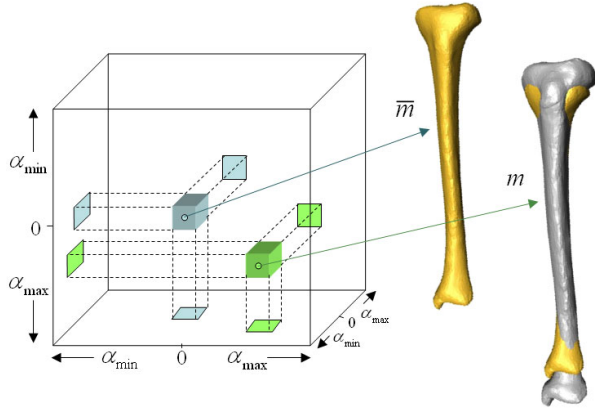
**Fig. 1**. Shape space defined by three first principal components. The center element (labeled in the figure $\bar{m}$) corresponds to the mean of the population. Each element in this shape space is formed by a linear combination of the principal components, in this example $m = \bar{m} + \alpha_1\sqrt{\lambda_1}\vec{u}_1 + \alpha_2\sqrt{\lambda_2}\vec{u}_2 + \alpha_3\sqrt{\lambda_3}\vec{u}_3$.

intensity-based nonrigid registration algorithm [10]. This algorithm defines the deformation on a uniformly-spaced grid and uses B-splines for interpolation between control points. The advantage of B-splines is that they are locally controlled, which makes them computationally efficient even for a large number of control points. The registration was performed in the combination of SSD (sum of square distances) similarity metric and gradient descent as optimisation function. Based on the deformation fields obtained from the registration process, we build vectors of corresponding positions and image intensities.

### 2.2. Principal Component Analysis

To reduce the dimensionality of the data, we apply PCA. PCA is a multivariate factor analysis technique aiming at finding a low-dimensional manifold in the space of the data, such that the distance between the data and its projection on the manifold is small [2]. PCA is the best, in the mean-square error sense, linear dimension reduction technique. The way to find the principal components is to compute the sample covariance matrix of the data set, $\vec{S}$, and then find its eigenstructure $\vec{S}\vec{U} = \vec{U}\vec{\Lambda}$. $\vec{U}$ is a $D \times D$ matrix which has the unit length eigenvectors $\vec{u}_1, ..., \vec{u}_D$ as its columns, and $\vec{\Lambda}$ is a diagonal matrix with the corresponding eigenvalues $\lambda_1, ..., \lambda_D$. The eigenvectors are the principal components and the eigenvalues their corresponding projected variances.

## 3. OPTIMISATION IN PCA SPACE USING LEVEL SETS

### 3.1. PCA shape space mapping

Let us consider the shape space defined by the weighted linear combination of the first $L \leq D$ eigenvectors $\vec{u}_1, ..., \vec{u}_L$ of the PCA decomposition of a set of training shapes in $\mathcal{R}^D$. Each element $m \in \mathcal{R}^D$ in this shape space is defined by a set of coefficients $\alpha_1, ..., \alpha_L$ (Figure 1):

$$m = \bar{m} + \sum_{i=1}^{L} \alpha_i \sqrt{\lambda_i}\vec{u}_i, \qquad (1)$$

where $\lambda_1, ..., \lambda_L$ are the eigenvalues corresponding to each principal component, and $\bar{m}$ is the arithmetic mean of the training sets. Now let us consider a scalar mapping $\mathcal{M} : A = [\alpha_{min}, \alpha_{max}]^L \rightarrow \mathcal{R}$. This mapping is intended to represent a clinically meaningful anatomical criterion derived from the shapes in the PCA space (e.g. femoral inclination angle [6]). We now would like to find all instances in the shape space that meet a certain criterion dependent on a scalar measure $\epsilon \in \mathcal{M}(A)$. This problem is approached as a segmentation in the PCA shape space defined by the mapping $\mathcal{M}$ defined above, and solved using the level sets framework described in the following section.

### 3.2. Level set segmentation

Segmentation techniques based on active contours, or deformable models, have been widely used in image processing for different medical applications [11, 12]. The idea behind active contours is to extract the boundaries of homogeneous regions within the image, while keeping the model smooth during deformation. A particular instantiation of this paradigm is that of active contours based on level sets [13].

Let us consider a parameterized closed surface $C(s) : S = [0,1]^{L-1} \rightarrow \mathcal{R}^L$ defined in a bounded region $\Omega \in \mathcal{R}^L$. In order to segment the observed image $\mu : \Omega \rightarrow \mathcal{R}$ we propose to minimize the following energy functional:

$$E(C) = a \int_\omega (\mu - \epsilon)\, \partial\Omega + b \int_S |C'|\, ds, \qquad (2)$$

where $\omega \subset \Omega$ and $C = \partial\omega$ is the closed surface. The first term represents the boundary force that attracts the evolving surface toward a predefined segmentation constraint $\epsilon = const$, while the second term regulates the smoothness of the surface. Here, $a$ and $b$ are positive scalar weights.

The segmentation algorithm is based on the implicit representation of deformable models implemented within the framework of level sets, and allows automatic change of topologies without reparametrization [14]. Using the level set formulation, the boundary surface $C = \partial\omega$ can be modeled as a zero level set of a Lipschitz function $\phi$, defined on the entire image domain $\Omega$ (Figure 2). By minimizing the energy functional with respect to $\phi$ we get a model associated Euler-Lagrange equation for boundary flow (see [6] for details):

$$\frac{\partial\phi}{\partial t} = a\,(\mu - M)\,\delta(\phi) + b\,div(\frac{\nabla\phi}{|\nabla\phi|})\,\delta(\phi). \qquad (3)$$

Thus, adopting the nomenclature of the previous section, $\mathcal{M}$ will be the $L$-dimensional "image" $\mu$ to be segmented, defined in the domain of shape coefficients $\Omega = A$. We emphasize again, that while level set segmentation techniques have been used in the object's geometry space, our aim is to use it in the parametric space of the statistical shape model.

### 3.3. Hierarchical approach to zero level set evolution

In order to decrease the computational complexity of the standard level set method we apply a hierarchical narrow band level set approach, which uses only the points close to the evolving front at every time step [15]. First we initialize our level set function using automatic seed initialisation on a low resolution shape space map. Then, minimisation of the energy functional 3 is performed
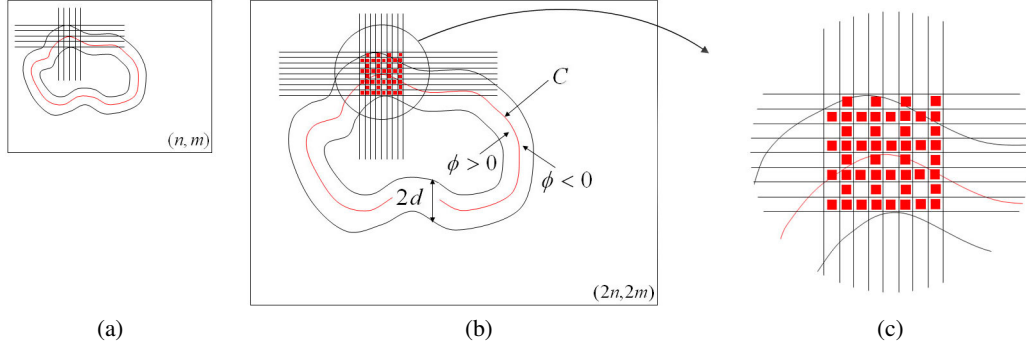
**Fig. 2**. Hierarchical approach to narrow band zero-level set evolution. (a) Initial low resolution PCA shape space map with a stable zero level set in red colour and a narrow band around it. (b) Higher-resolution map with the augmented narrow band and zero level set, adopted from the low-resolution map. (c) The values of white pixels in the grid map come from the low resolution map, while the values of the red pixels that come from the augmented map still need to be calculated.

to evolve the surface towards the segmented region. The seed initialization consists of partitioning the data image $u_0$ into $N$ windows $W_n$, $n = 1..N$ of predefined size.

We define a thin band around the zero-level set that contains the neighboring points with distance to the zero-level less than $d_{max}$. The level set is then updated only on these points, instead of re-calculating it for each grid point (Figure 2). As the zero-level set corresponding to the front evolves, we must ensure that it stays within the band. For this, we re-initialize the band after 10 iterations, when the front is close to the edge of the domain, using the current zero-level set as the initial surface. Once the stable boundaries of the low resolution map are reached we increase the resolution of the shape space and continue zero-level set surface evolution in the augmented low-resolution narrow band.

## 4. IMPLEMENTATION AND RESULTS

We present results obtained from a training set of tibia surface models extracted from CT data. The training set consists of 92 left human tibia from which Asian, Caucasian, male and female are equally present. Statistical shape model was then computed, as explained in Section 2. We retain the first five principal components which account for 92% of shape variability in the population. Using more than five modes to explain the statistical model would give us more subtle changes which, however, do not bring modifications in the area of implant placement (Figure 3). We define the mapping transformation $\mathcal{M}$ as the mean error distance from 844 points on the implant surface to the best fitted points on the bone surface. The PCA shape space is then built by sampling the space of shape coefficients, generating the corresponding shape, and then computing the mapping $\mathcal{M}$ to obtain the measure of interest. We use the range $-3 \leq \alpha_i \leq 3$ for every shape coefficient. This accounts for 99.7% of the shape variability encompassed in each principal component.

We apply our method to evaluate performance of orthopaedic implant. A modified Iterative Closest Point (ICP) technique, developed in our group for the specific task of bone implant fitting [16], was used to compute the scalar mapping. In this work, a collision constraint was incorporated to ensure that no points in the implant mesh model fall inside the bone model. In addition, fitting guidelines provided by the implant manufacturer were included as fitting constraints, to favor fittings of the implant that are collinear with the bone main axis, and do not take place above the bone plateau. Figure 4 shows the initialisation step of the automatized implant fitting
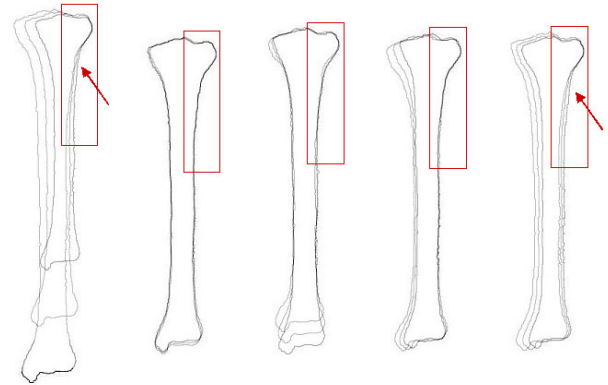


**Fig. 3**. The first five modes of variation for the left human tibia: $\bar{m} - 3\sqrt{\lambda_i}\vec{u}_i, \bar{m}, \bar{m} + 3\sqrt{\lambda_i}\vec{u}_i$, for $i = 1..5$. The arrows point to the area of implant placement, which is most affected by first and fifth principal component.

procedure and the final result of the fitting where the colour map of the implant represents the distance map of the fitting error. We start with a low dimension map 60x60 and we initialise the zero level set by applying seed initialisation on the PCA shape space, and then we proceed with hierarchical zero level set, as explained in Section 3.3. We do not need to explicitly compute mean error fitting, for every point in the shape space, but only in a narrow band around the zero level set. We continue with a hierarchical narrow band approach by augmenting our space to dimensions 120x120 and 240x240. Narrow band level set approach is mandatory to decrease high computation times and to reduce the search space of shape parameters.

The segmented areas in Figure 5a and Figure 5b represent the range of parametric values that generate tibia shapes satisfying the given segmentation criterion $\epsilon$, i.e. that best fit to the given implant, with a fitting error of $\epsilon = 0.8mm$ and $\epsilon = 1mm$ respectively. Figure 5c shows an example of a construction of a 3D PCA shape space (i.e. using 3 principal components to generate the shape instances) and the result of the level set optimisation for the fitting error less then 1mm. We decided to exclude principal components $u_3$ and $u_4$ since their variations do not affect the bone in the area of the implant placing (Figure 3). It can be seen in Figure 5 that the result of the
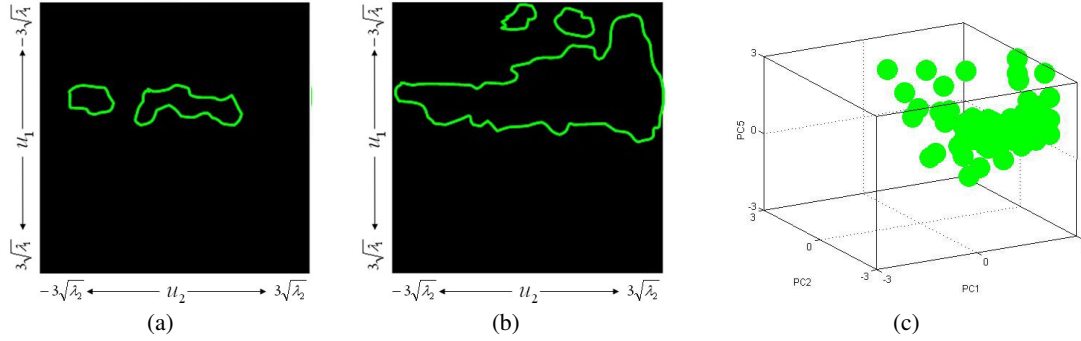
**Fig. 5**. Automatic hierarchical 2D level set segmentation gives the spectrum of shapes that have fitting error less than (a) 0.8mm, and (b) 1mm. (c) 3D level set segmentation gives the spectrum of shapes that have the fitting error less than 0.8mm.
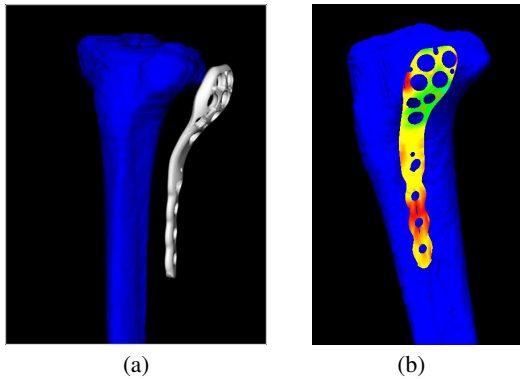


**Fig. 4**. (a) The initialisation of the implant fitting. (b) The final result of the implant fitting shows the distance map of fitting error, where the red colour represents the perfect fitting of the implant to the bone and the green colour represents the distance of 3mm to the bone surface.

fitting is much more dependable on the first principal component, as the segmented area falls in the negative values of $u_1$. It can be concluded that changes of the length of tibia bone affect the result of the fitting, as do changes of the oblique line of tibia and a slight torsion of the lateral surface of the tibia.

## 5. CONCLUSIONS AND FUTURE WORK

Current evaluation and optimisation of the implant is done by manual fitting and fixation procedures, applied on a small set of cadaver bones in a trial-and-error process to find the optimal shape and mechanic properties. The method that we propose allows to virtually test the implants on a representative set of bones, generated by sampling the statistical model, and to optimise implant shape as to fit a maximum of the target population. Hence, our result is of great importance for the implant manufacturer. Ongoing work includes the correlation of the principal components to the given implant geometry, so that the modifications to the implant design/geometry could be assessed directly from the segmented map.

## 6. REFERENCES

[1] TF Cootes et al, "Active shape models - their training and applications," *Comput. Vis. Image Underst.*, vol. 61, no. 1, pp. 38–59, 1995.

[2] C Bishop, *Neural Networks for Pattern Recognition*, Oxford University Press, USA, 1995.

[3] TF Cootes et al, "Anatomical statistical models and their role in feature extraction," *Br. J. Radiol.*, vol. 77, pp. S133–S139, 2004.

[4] MG Roberts et al, "Automatic segmentation of lumbar vertebrae on digitised radiographs using linked active appearance models," in *Proc. MIUA*, 2006, pp. 120–124.

[5] R Sierra et al, "Generation of variable anatomical models for surgical training simulators," *Med. Image Anal.*, vol. 10, no. 2, pp. 275–285, 2006.

[6] N Kozic et al, "Statistical shape space analysis based on level sets," in *Proc. MIAR*, 2008, pp. 160–167.

[7] D Cremers, "Dynamical statistical shape priors for level set based tracking," *IEEE Trans. Pattern Anal. Mach. Intell.*, vol. 28, no. 8, pp. 1262–1273, 2006.

[8] M Leventon et al, "Level set based segmentation with intensity and curvature priors," in *Proc. IEEE Workshop on Mathematical Methods in Biomedical Image Analysis*, 2000, pp. 4–11.

[9] M Rousson et al, "Implicit active shape models for 3D segmentation in MRI imaging," *Proc. MICCAI*, pp. 209–216, 2004.

[10] D Rueckert et al, "Automatic construction of 3D statistical deformation models of the brain using non-rigid registration," *IEEE Trans. Med. Imaging*, vol. 22, no. 8, pp. 1014–1025, 2003.

[11] M Kass et al, "Snakes: Active contour models," *Int. J. Comput. Vis.*, vol. 1, no. 4, pp. 321–331, 1987.

[12] T McInerney et al, "Deformable models in medical image analysis: A survey," *Med. Image Anal.*, vol. 1, no. 2, pp. 91–108, 1996.

[13] TF Chan et al, "Active contours without edges," *IEEE Trans. Image Process.*, vol. 10, no. 2, pp. 266–277, 2001.

[14] S Osher et al, "Fronts propagating with curvature-dependent speed: Algorithms based on Hamilton-Jacobi formulation," *J. Comput. Phys.*, vol. 79, pp. 12–49, 1988.

[15] D Adalsteinsson et al, "A fast level set method for propagating interfaces," *J. Comput. Phys.*, vol. 118, pp. 269–277, 1995.

[16] M Reyes et al, "Evidence-based implant design using a statistical bone model and automated implant fitting," in *Proc. CAOS*, 2008, pp. 379–381.